ASME Journal of Tribology
Online journal at:
https://asmedigitalcollection.asme.org/tribology

Shubo Zhang[1]
School of Chemistry, Chemical Engineering and Biotechnology,
Nanyang Technological University,
Singapore 637457
e-mail: shubo002@e.ntu.edu.sg

Michele Ciavarella
DMMM Department,
Politecnico di BARI,
Viale Gentile 182, Bari 70126, Italy;
Department of Mechanical Engineering,
Hamburg University of Technology,
Am Schwarzenberg-Campus 1,
Hamburg 21073, Germany
e-mail: m.ciavarella@poliba.it

Static Friction Coefficient Depends on Geometry

Classical theories state that the friction coefficient is independent of geometry, depending only on the real contact area determined by roughness. However, experimental evidence shows significant differences between static and dynamic friction coefficients. Recent models introduce an energetic theory for friction, analogous to the Griffith theory for fracture, resulting in a constant dynamic friction coefficient at heavy loads but a larger static coefficient at low loads. We show that, for power-law punches, the ratio of static to dynamic friction coefficients at low normal loads is higher for flatter profiles and, in principle, grows unbounded at zero load. This may explain the observed variability in friction ratios. The model's predictions align well with recent experimental results.
[DOI: 10.1115/1.4070853]

Keywords: friction, tribology, fracture, interfacial energy, power-law punch, contact area, contact mechanics

1 Introduction

Friction is a ubiquitous phenomenon presented at interacting interfaces in relative motion, spanning from the atomic scale to earthquake faults extending over thousands of kilometers. The classical laws of friction, initially proposed by Amontons and Coulomb (if not Leonardo da Vinci), state that the friction force is proportional to the normal load, but independent of the shape of the contacting bodies.[2] The distinction between static and dynamic (or kinetic) friction coefficients was later proposed by Euler through experiments using inclined planes, by means of the observation that just above the critical angle of static friction, the velocity of the sliding solid is not very small because of the dynamic friction reduction. Rabinowicz [2] conducted more systematic experiments, attributing to the reduction of friction in the transition from stick to sliding to the interfacial energy of metals and providing a method to measure this frictional energy. In particular, by impacting a small ball of mass m_0 into a stationary block of mass M_0, a critical distance is found such that the block is set into motion right down the plane, and this is related to the frictional energy. Although the difference between static and dynamic coefficients of friction is generally minor for dry metals, in some cases, it has been reported also quite high, although the references do not show when this difference was large (see, e.g., the RoyMech database[3]). In the mechanics of earthquake faults, this difference has been reported to reach values as high as 10, prompting Rice to refer to such interfaces as "strong but brittle" [3].

The concept of fracture mechanics was introduced into contact mechanics for the study of adhesion and friction as early as the 1970s [4–8], in particular for friction providing valuable explanations for failures where the shear stress does not reach the expected limiting strength throughout. Studies on natural faults typically revert to fracture mechanics, where the slip-weakening law represents a simplified case compared with more elaborate friction laws, such as the rate-state law [9,10], which, however, is still under debate owing to numerous variants. Energy-based model of friction also suggests a size effect in frictional behavior [11,12].

In continuum mechanics models based on the Amontons–Coulomb law, the Cattaneo–Mindlin model assumes the geometry of a Hertzian contact to address the quasi-static stick-slip transition [13,14]. Under the full-stick assumption, the model necessitates a singular shear stress at the contact boundary, while the normal pressure approaches zero, thus leading to an unbounded friction coefficient and violating the Amontons–Coulomb law. Consequently, the classical Cattaneo–Mindlin model identified shear traction through a clever superposition of a full-slip solution with a correction term, the latter enforcing the boundary condition of constant tangential displacement. This is akin to a shear analog of the Dugdale–Barenblatt cohesive zone model in fracture mechanics [15,16]: The "cohesive" (slip) zone is subjected to the tangential stress, which relieves the shear stress concentration at the "crack tip" (the stick zone edge). This result was extended by Ciavarella and Jäger to arbitrary geometries [17–19], highlighting that the correction term within the stick zone is always proportional to the pressure distribution for a correspondingly reduced normal load. Similar results were also introduced for harmonic loadings with more complicated superpositions [20]. The classic Cattaneo–Mindlin solution has a single value of friction coefficient given by the Amontons–Coulomb law. Although the fracture mechanics-based approaches have proven highly effective in addressing adhesion–friction coupling problems [4,8,21,22], our primary interest lies in scenarios where surface roughness suppresses adhesion—such as in hard bodies where roughness is insufficient to disrupt frictional energy.

To resolve the quasi-static transition from stick to slip, the Griffith fracture model [23] and the classical singular solutions for

[1]Corresponding author.
[2]Leonardo suggested that friction coefficient should be universal and close to 0.24, a value that curiously has been found as a universal limit for granular media recently [1].
[3]http://www.roymech.co.uk/Useful_Tables/Tribology/co_of_frict.htm#coef
Contributed by the Tribology Division of ASME for publication in the JOURNAL OF TRIBOLOGY. Manuscript received October 1, 2025; final manuscript received January 6, 2026; published online February 6, 2026. Assoc. Editor: Yang Xu.

shear cracks in fracture mechanics were applied to the frictional contact problem for a spherical geometry by Ciavarella [24]. This model indicates a sudden transition to slip when the stick zone reduces to a certain critical size relative to the overall contact area. The static friction coefficient observed prior to sliding can be significantly higher than the kinetic friction coefficient, governed by an elastic instability analogous to the pull-off instability in adhesive contacts. Additionally, for a given frictional fracture energy, it implies that the static friction coefficient depends on the specimen size and normal load, while the dynamic friction remains constant.

Recently, Peng et al. [25] reported very detailed experiments observing static-to-dynamic friction ratio reduction as normal load increases to the transition from single-asperity to multi-asperity contact interfaces. They observed that below a certain normal load threshold, the macroscopic friction coefficient becomes independent of the normal load. This is explained as friction behavior reverting to measurements at the nanoscale by atomic force microscopy (AFM) under single-asperity contact limits. They modeled this behavior by accurately characterizing surface roughness and using a simple frictional model with two parameters—static and dynamic friction coefficients—both inferred experimentally. Although this model effectively reproduces experimental observations, it relies on AFM measurements and a full numerical implementation. By contrast, Ciavarella [26] modeled the drop of friction coefficients ratio also using two parameters—a dynamic friction coefficient and a friction energy—both extrapolated from macroscopic experiments. This approach offers the advantage of a closed-form analytical formulation. The friction ratio drop with increasing normal load for the case of soft materials with macroscopic adhesion is also predicted by Xu et al. [27] using an adhesive friction model for rough surface contact.

In this article, we extend a modified Cattaneo–Mindlin model incorporating Griffith–type friction by accounting for the influence of surface roughness through a fracture energy that varies linearly with local contact pressure. We predict that at low normal loads, the ratio of static to dynamic friction coefficients reaches a value that is strongly affected by the contact geometry, although eventually there is divergence to infinite coefficient at zero load. This provides a plausible explanation for the experimentally observed difference between static and dynamic friction coefficients.

2 The Model

Consider an axisymmetric punch in contact with a substrate under a normal load P and subjected to a tangential load Q, as shown in Fig. 1(*a*). Within the contact area A of radius a, in addition to the pressure distribution $p(x, y)$, frictional shear stress $q(x, y)$ will be present to balance the tangential load Q.

2.1 The Friction Model With Griffith Theory. The basic idea of Cattaneo–Mindlin superposition [13,14] is to find a shear stress distribution such that the displacement in the stick zone becomes constant, and only outside the stick zone, the relative motion happens, as prescribed by congruence of displacements. Therefore, the friction in the slip zone would follow the Amontons–Coulomb law with dynamic friction coefficient f, but the friction inside the stick zone is required to have a correction term $q^*(x, y)$. The friction stress distribution can be expressed as follows:

$$\begin{aligned} q(x, y) &= fp(x, y) - q^*(x, y); \quad (x, y) \in A_{\text{stick}} \\ q(x, y) &= fp(x, y); \quad (x, y) \in A_{\text{slip}} \end{aligned} \tag{1}$$

where A_{stick} denotes the region without relative slip and A_{slip} denotes the region where relative displacement occurs. The global loads will be related by

$$Q = fP - Q^* = f(P - P^*) \tag{2}$$

where $P^* = Q^*/f$ represents the correction term in the stick zone given by the Cattaneo–Mindlin model. In the spherical indenter example, by analogy with fracture mechanics, the correction term includes a singular shear stress at the stick-slip boundary $r = c$ [24]:

$$q^*(r) = f\left[q_0\sqrt{1-\left(\frac{r}{c}\right)^2} - \frac{q_0'}{\sqrt{1-\left(\frac{r}{c}\right)^2}}\right], \quad r < c \tag{3}$$

which has a similar form of pressure distribution as that in the Johnson–Kendall–Roberts (JKR) theory [4]. In this case, we denote the correction load as P^*_{JKR} as follows:

$$P^*_{\text{JKR}} = P^*_{\text{AL}} - P^*_{\text{A}} \tag{4}$$

where P^*_{AL} and P^*_{A} represent the adhesiveless and adhesive normal load by analogy with the JKR solution [4], respectively. It should be emphasized that, although the mathematical form is almost identical to that of the JKR theory [4], this model is derived for shear traction instead of pressure distribution. Accordingly, the condition for the shear traction distribution at the edge of the stick-slip zone is that the mode-II energy release rate G_{II} reaches a critical value G_c, which corresponds to the frictional fracture energy γ defined later in this article. For example, consider a sphere punch of

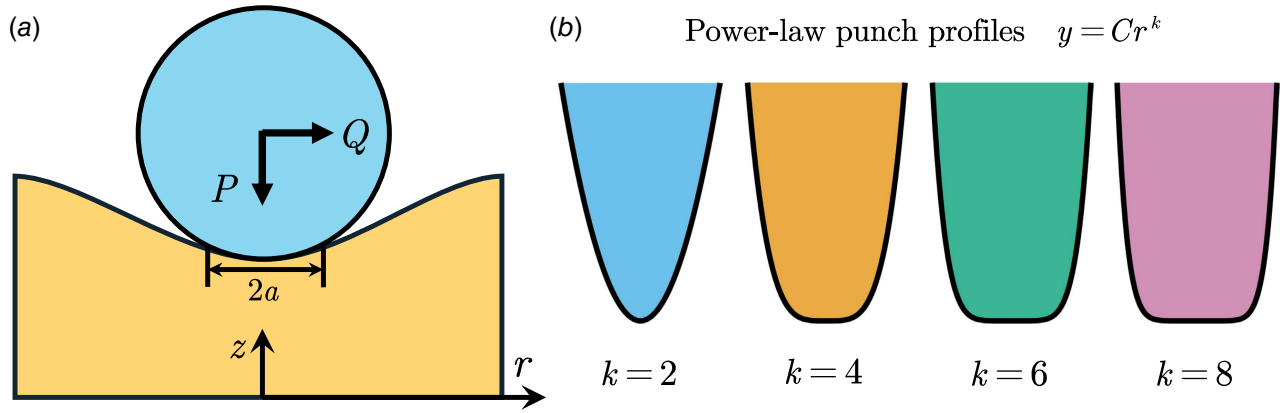

Fig. 1 Schematic of the model. (*a*) A three-dimensional axisymmetric (or two-dimensional) rigid punch is brought into contact with a substrate under an external load. The normal component of the load *P* produces a contact region *A* with radius *a*. The tangential component of the load *Q* gives rise to frictional shear stress within the contact area. (*b*) The shapes of power-law punches used in this study.

radius R in contacting with a plane substrate. The composite modulus E^* is defined as follows:

$$\frac{1}{E^*}=\frac{1-\nu_1^2}{E_1}+\frac{1-\nu_2^2}{E_2} \tag{5}$$

where E_1 and E_2 are the Young's modulus, and ν_1 and ν_2 are the Poisson's Ratio of contacting bodies. The corrective load $P^*_{\mathrm{AL}}=4E^*c^3/3R$ in the Hertzian case and the adhesive term $P^*_{\mathrm{A}}=\sqrt{16\pi\gamma E^*c^3}$ for 3D axisymmetric case, where γ is the frictional surface energy, are applied via Eqs. (2) and (4) to the global friction coefficient:

$$\frac{f_s}{f}=\left(\frac{|Q|}{fP}\right)_{\max}=1-\frac{P^*_{\mathrm{JKR}}}{P} \tag{6}$$

It is noted that in Eq. (6), the normal load P depends solely on the contact radius a, whereas P^*_{JKR} is associated with the stick zone radius c. Hence, for a given normal load, we define the stick zone radius corresponding to the maximum friction force as the critical radius c_c.

2.2 The Pressure-Dependent Friction Energy. It has been suggested that the frictional fracture energy directly depends on the real contact area for rough surface contact, which is governed by the normal load and constitutes only a small fraction of the nominal contact area [28]. As the normal pressure increases, more asperities coming into contact enlarges the real contact area, thereby enhancing the frictional fracture energy. Alternatively to the real contact area explanation, Papangelo et al. [22] observe that the friction fracture energy in a cohesive model perspective is the integral of the shear traction as a function of the slip displacement, and shear traction is proportional to the friction coefficient at the given slip displacement and the pressure. Hence, the variation of the frictional fracture energy along the stick-slip boundary is given as follows:

$$\gamma'=\frac{p(c)}{p_{0,\mathrm{ref}}}\gamma_{\mathrm{ref}} \tag{7}$$

where $p(c)$ is the pressure at the stick-slip boundary, $p_{0,\mathrm{ref}}$ is the reference pressure at the contact center, and γ_{ref} is the arbitrarily chosen reference friction energy at the reference pressure. This has found validation against the experiments [25] by Ciavarella [26]. In the following derivation, we will choose appropriate corresponding reference load P_{ref} for the simplicity of the expression. To avoid potential confusion, all quantities corrected for pressure dependence in this article will be denoted with a prime ($'$).

3 Solution to Partial Slip Contact

3.1 The Three-Dimensional Solution

3.1.1 Hertzian Sphere Contact. The frictional force for the Hertzian contact is given by Eq. (17) in the previous study [24]:

$$\frac{Q}{fP}=1-\left(\frac{c}{a}\right)^3\left[1-2\left(\frac{c_c}{a}\frac{a}{c}\right)^{3/2}\right] \tag{8}$$

where c_c is the constant such that

$$\frac{c_c}{a}=\sqrt[3]{\frac{3\pi\gamma R}{P}} \tag{9}$$

The friction ratio f_s/f is given by its peak value at $c=c_c$:

$$\left(\frac{|Q|}{fP}\right)_{\max}=1+\left(\frac{c_c}{a}\right)^3=1+\frac{3\pi\gamma R}{P} \tag{10}$$

According to Eq. (7), the pressure-dependent friction energy in Hertzian contact is given as follows:

$$\gamma'=\frac{p_0}{p_{0,\mathrm{ref}}}\gamma_{\mathrm{ref}}\sqrt{1-\left(\frac{c}{a}\right)^2} \tag{11}$$

Replacing Eq. (11) into Eq. (9) yields

$$\begin{aligned}\frac{c_c^*}{a}&=\sqrt[3]{\frac{3\pi\gamma' R}{P}}=\sqrt[3]{\frac{3\pi\gamma_{\mathrm{ref}}R}{P}\frac{p_0}{p_{0,\mathrm{ref}}}\sqrt{1-\left(\frac{c}{a}\right)^2}}\\&=\left(\frac{P_{\mathrm{ref}}}{P}\right)^{2/9}\left[1-\left(\frac{c}{a}\right)^2\right]^{1/6}\end{aligned} \tag{12}$$

where $P_{\mathrm{ref}}=3\pi\gamma_{\mathrm{ref}}R$ and $(p_0/p_{\mathrm{ref}})^3=P/P_{\mathrm{ref}}$.[4] Replacing c_c/a in Eq. (8) with Eq. (12), we have Q/fP as a function of c/a (with a single parameter P/P_{ref}):

$$\frac{Q}{fP}=1-\left(\frac{c}{a}\right)^3+2\left(\frac{P_{\mathrm{ref}}}{P}\right)^{1/3}\left[1-\left(\frac{c}{a}\right)^2\right]^{1/4}\left(\frac{c}{a}\right)^{3/2} \tag{13}$$

The friction force distribution Q/fP after pressure-dependent correction reaches its maximum value (i.e., the friction ratio) at the corrected critical radius c_c', which can be numerically solved by taking extremum point from Eq. (13):

$$\frac{\mathrm{d}}{\mathrm{d}c}\left(\frac{Q}{fP}\right)=0 \tag{14}$$

3.1.2 Axisymmetric Power-Law Punches. Consider a punch with power-law profile given by $g_0(r)=Cr^k$ as shown in Fig. 1(*b*). When a normal load P is applied, the applied force is related to the contact radius a by $P=E^*Cka^{k+1}\mathrm{B}(k/2+1,1/2)$ (see the Appendix), where E^* is the composite modulus. The adhesiveless correction term should have the same form as the normal load, but with the contact radius a replaced by the stick zone radius c as follows:

$$P^*_{\mathrm{AL}}=E^*Ckc^{k+1}\mathrm{B}\left(\frac{k}{2}+1,\frac{1}{2}\right) \tag{15}$$

The corresponding adhesive correction term is $P^*_{\mathrm{A}}=\sqrt{16\pi\gamma E^*c^3}$. By substituting the power-law punch solution into the load expression Eq. (4) and normalizing by the normal load, we obtain

$$\frac{P^*_{\mathrm{JKR}}}{P}=\frac{P^*_{\mathrm{AL}}-P^*_{\mathrm{A}}}{P}=\left(\frac{c}{a}\right)^{k+1}-\frac{\sqrt{16\pi\gamma E^*c^3}}{E^*Cka^{k+1}B\left(\frac{k}{2}+1,\frac{1}{2}\right)} \tag{16}$$

The critical size of the stick zone c_c is attained when the corrective load P^*_{JKR} reaches its maximum:

$$c_c^{k-\frac{1}{2}}=\frac{3M}{2(k+1)},\quad \text{where } M=\frac{\sqrt{16\pi\gamma E^*}}{E^*CkB\left(\frac{k}{2}+1,\frac{1}{2}\right)} \tag{17}$$

We normalize the critical radius c_c using power-law punch solution Eq. (A1) as follows:

$$\frac{c_c}{a}=\frac{1}{P^{\frac{1}{k+1}}}\left[\frac{3\sqrt{16\pi\gamma E^*}}{2(k+1)}\right]^{\frac{2}{2k-1}}\left[\frac{1}{E^*CkB\left(\frac{k}{2}+1,\frac{1}{2}\right)}\right]^{\frac{3}{(k+1)(2k-1)}} \tag{18}$$

By using Eqs. (16) and (18), the ratio of apparent static coefficient over the dynamic one can be written as follows:

$$\frac{Q}{fP}=1-\frac{P^*_{\mathrm{JKR}}}{P}=1-\left(\frac{c}{a}\right)^{k+1}\left[1-\frac{2(k+1)}{3}\left(\frac{c_c}{a}\frac{a}{c}\right)^{k-1/2}\right] \tag{19}$$

[4]Note that c_c^* denotes the corrected value of c_c, where we applied the pressure-dependent fracture energy γ' instead of the constant value γ, but does not refer to the corrected extremum point.

The first estimation of friction coefficients ratio is attained at $c = c_c$:

$$\left(\frac{|Q|}{fP}\right)\Big|_{\max} = 1 + \frac{2k-1}{3}\left(\frac{c_c}{a}\right)^{k+1} = 1 + \frac{2k-1}{3}\cdot\frac{P_{\text{ref}}}{P} \tag{20}$$

where P_{ref} includes constants in Eq. (18). The pressure-dependent frictional energy can be written as follows using Eqs. (A1) and (A3)

$$\gamma' = \gamma_{\text{ref}}\frac{p_0}{p_{0,\text{ref}}}m_{k,3D}\left(\frac{c}{a}\right) = \gamma_{\text{ref}}\left(\frac{P}{P_{\text{ref}}}\right)^{\frac{k-1}{k+1}}m_{k,3D}\left(\frac{c}{a}\right) \tag{21}$$

where $m_{k,3D}(s)$ describes the pressure distribution over the stick area and is given by Eq. (A4). By substituting Eq. (21) into Eq. (18), we have

$$\frac{c_c^*}{a} = \left(\frac{P_{\text{ref}}}{P}\right)^{\frac{k}{(k+1)(2k-1)}}\left[m_{k,3D}\left(\frac{c}{a}\right)\right]^{\frac{1}{2k-1}} \tag{22}$$

By replacing c_c/a in Eq. (19) with Eq. (22), we obtain

$$\frac{Q}{fP} = 1 - \left(\frac{c}{a}\right)^{k+1} + \frac{2(k+1)}{3}\left(\frac{P_{\text{ref}}}{P}\right)^{\frac{k}{2(k+1)}}\left[m_{k,3D}\left(\frac{c}{a}\right)\right]^{1/2}\left(\frac{c}{a}\right)^{3/2} \tag{23}$$

3.1.3 Results. In Fig. 2, we plot the change of critical stick zone radius c_c' with increasing normal load P. It is shown that most of the contact area constitutes the stick zone at slight normal load, i.e., $\lim_{P\to 0}(c_c'/a) > 0.8$, and the proportion of the critical region within the contact area decreases as the normal load increases.

The comparison of friction drop as a function of normal load is reported in Fig. 3 without (dashed line) and with (solid line) the pressure-dependent correction for $k = 2, 4, 6, 8$ ($k = 2$ is also referred as Hertzian). The ratio of friction coefficients at small normal loads is significantly decreased when pressure-dependent corrections are taken into account, but it remains true that flatter geometries have greater static friction.

3.2 The Two-Dimensional Solution

3.2.1 Hertzian Cylinder Contact. The frictional force for the 2D Hertzian contact is given by equation (47) in the previous paper [21]:

$$\frac{Q}{fP} = 1 - \left(\frac{c}{a}\right)^2\left[1 - 4\left(\frac{c_c}{a}\frac{a}{c}\right)^{3/2}\right] \tag{24}$$

where c_c is the extremum point such that

$$\frac{c_c}{a} = \sqrt[6]{\frac{\pi R E^*}{16}}\cdot\frac{\gamma^{1/3}}{P^{1/2}} \tag{25}$$

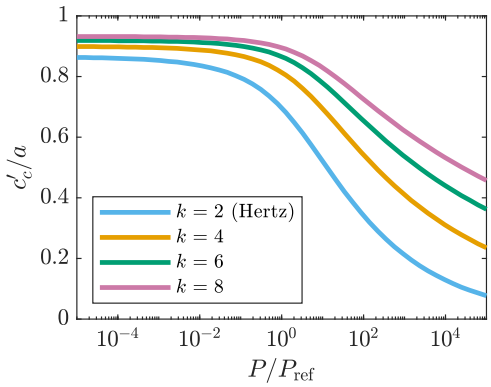

Fig. 2 The critical stick zone radius c_c'/a corrected for pressure-dependent friction energy as a function of normal load P for 3D axisymmetric power-law punches

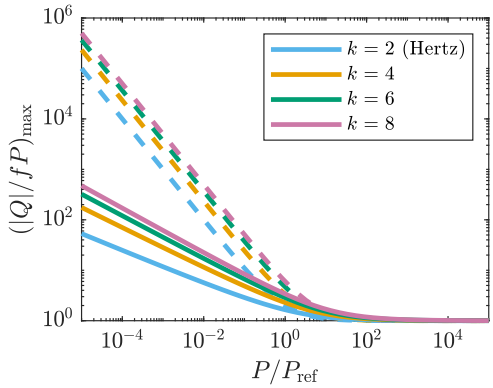

Fig. 3 Friction drop as a function of normal load without pressure dependency (dashed line) versus with pressure-dependent correction (solid line) for 3D axisymmetric power-law punches

The maximum friction coefficients ratio is reached at $c = c_c$:

$$\left(\frac{|Q|}{fP}\right)_{\max} = 1 + 3\left(\frac{c_c}{a}\right)^2 = 1 + \frac{3}{P}\sqrt[3]{\frac{\pi E^* R\gamma^2}{16}} \tag{26}$$

However, the frictional fracture energy γ is considered as a constant. The pressure-dependent friction energy for 2D Hertzian contact is given as follows:

$$\gamma' = \frac{p_0}{p_{0,\text{ref}}}\gamma_{\text{ref}}\sqrt{1 - \left(\frac{c}{a}\right)^2} = \gamma_{\text{ref}}\left(\frac{P}{P_{\text{ref}}}\right)^{1/2}\sqrt{1 - \left(\frac{c}{a}\right)^2} \tag{27}$$

where we applied $(p_0/p_{0,\text{ref}})^2 = P/P_{\text{ref}}$ for the 2D Hertzian contact. By substituting Eq. (27) into Eq. (25) and choosing the appropriate reference load P_{ref}, we obtain

$$\frac{c_c^*}{a} = \left(\frac{P_{\text{ref}}}{P}\right)^{1/3}\sqrt[6]{1 - \left(\frac{c}{a}\right)^2} \tag{28}$$

Equation (24) is revised accordingly

$$\frac{Q}{fP} = 1 - \left(\frac{c}{a}\right)^2 + 4\left(\frac{P_{\text{ref}}}{P}\right)^{1/2}\sqrt[4]{1 - \left(\frac{c}{a}\right)^2}\left(\frac{c}{a}\right)^{1/2} \tag{29}$$

3.2.2 Power-Law Punches. For a 2D power-law punch with profile $g_0(x) = C|x|^k$, Papangelo and Ciavarella [21] reported the friction force as follows:

$$\frac{Q}{fP} = 1 - \left(\frac{c}{a}\right)^k\left[1 - 2k\left(\frac{c_c}{a}\frac{a}{c}\right)^{k-1/2}\right] \tag{30}$$

and the corresponding friction ratio as follows:

$$\left(\frac{|Q|}{fP}\right)_{\max} = 1 - (1-2k)\left(\frac{c_c}{a}\right)^k \tag{31}$$

where the critical radius as follows:

$$c_c = \left[\frac{1}{kC}\sqrt{\frac{\gamma}{2E}}\frac{\Gamma\left(\frac{k}{2}\right)}{\Gamma\left(\frac{k+1}{2}\right)}\right]^{\frac{1}{k-1/2}} \tag{32}$$

The contact radius with respect to the normal load is given by

$$a = \sqrt[k]{\frac{2P}{CkE\sqrt{\pi}}\frac{\Gamma\left(\frac{k}{2}+1\right)}{\Gamma\left(\frac{k+1}{2}\right)}} \tag{33}$$

To apply the pressure-dependent friction energy correction, we assume

$$\gamma' = \frac{p_0}{p_{0,\text{ref}}}\gamma_{\text{ref}}m_{k,2D}\left(\frac{c}{a}\right) \tag{34}$$

where $m_{k,2D}(s)$ is the Gauss hypergeometric function of argument s^2:

$$m_{k,2D}(s) = \frac{1}{\sqrt{\pi}}\left[\frac{\Gamma\left(\frac{k-1}{2}\right)}{\Gamma\left(\frac{k}{2}\right)}\,{}_2F_1\left(1, 1-\frac{k}{2}; \frac{3-k}{2}; s^2\right)\right.$$
$$\left.\cdot\sqrt{1-s^2} + \sqrt{\pi}|s|^{k-1}\tan\left(\frac{k\pi}{2}\right)\right]$$

The 2D power-law punch load and pressure have the form $P \propto a^k$ and $p_0 \propto a^{k-1}$ [21], and hence, we have $(p_0/p_{0,\text{ref}})^k = (P/P_{\text{ref}})^{k-1}$. By substituting Eq. (34) into Eq. (32) and dividing by Eq. (33), we obtain

$$\frac{c_c^*}{a} = \left(\frac{P_{\text{ref}}}{P}\right)^{\frac{1}{2k-1}}\left[m_{k,2D}\left(\frac{c}{a}\right)\right]^{\frac{1}{2k-1}} \tag{35}$$

Equation (30) is revised accordingly

$$\frac{Q}{fP} = 1 - \left(\frac{c}{a}\right)^k + 2k\left[\frac{P_{\text{ref}}}{P}m_{k,2D}\left(\frac{c}{a}\right)\frac{c}{a}\right]^{1/2} \tag{36}$$

3.2.3 Results. The corrected critical radius c_c' is shown in Fig. 4. It is shown that part of the contact area becomes the stick zone at very small normal load, which is quite similar to that of the 3D axisymmetric case, but it has a smaller limiting value.

To compare friction drop as a function of normal load, we plot in Fig. 5 both the solution without (dashed line) and with (solid line) the pressure-dependent correction for $k = 2, 4, 6, 8$ ($k = 2$ is also referred as Hertzian). Slightly different from the 3D axisymmetric case, the friction coefficients decreases less than 3D case when friction energy pressure dependency is considered.

3.3 Experimental Validation. By capturing the results of the friction drop by Peng et al. [25] as a function of normal load, we report in Fig. 6 the experimental data (mean values, scatter is also due to tests involving three sets of roughness) with 100 s (yellow dots, $P_{\text{ref}} = 0.18$ mN) and 10 s (green dots, $P_{\text{ref}} = 0.08$ mN) holding time, and with blue continuous line, the result from the present model for 3D Hertzian punch. The blue dashed line represents the prediction without pressure-dependent correction. The experimental data are fitted in the same way as that by Ciavarella [26]. Notice that there is a set of data [25] with less holding time (10 s) before applying frictional force, which corresponds to a smaller real contact area. Hence, in accord to our pressure-dependent theory, the friction energy is expected to be smaller, and accordingly, it is correct to expect smaller static friction coefficient, as found in experiments.

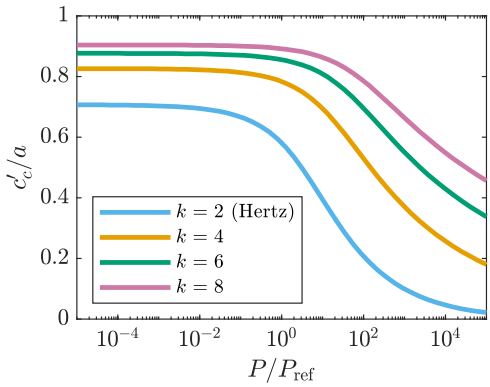

Fig. 4 The critical stick zone radius c_c'/a corrected for pressure-dependent friction energy as a function of normal load P for 2D power-law punches

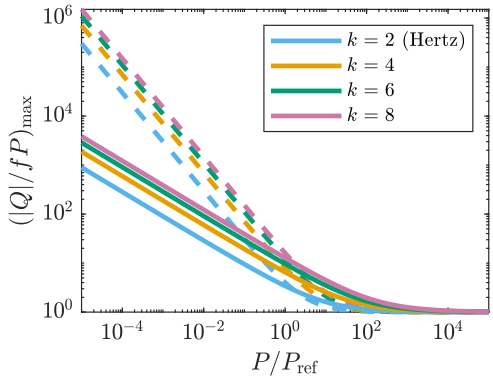

Fig. 5 Friction drop as a function of normal load without pressure-dependent (dashed line) versus with pressure-dependent correction (solid line) for 2D power-law punches

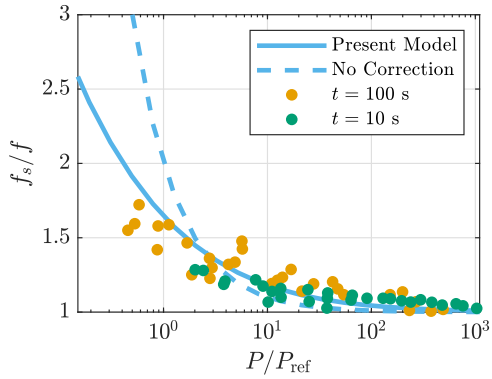

Fig. 6 Friction drop as a function of normal load P with different holding time t as given in the study by Peng et al. [25] versus 3D Hertzian punch with (solid line) and without (dashed line) pressure-dependent friction energy with fitted $P_{\text{ref}} = 0.18$ mN for $t = 100$ s and $P_{\text{ref}} = 0.08$ mN for $t = 10$ s

4 Discussion

Inspired by the ideas presented by Ciavarella [24], the present model further extends the results of Papangelo and Ciavarella [21], which is validated by experimental observations by Peng et al. [25] as shown in Fig. 6. We compare the friction reduction of indenters with different profiles in three-dimensional axisymmetric and two-dimensional cases. By considering the pressure dependence of fracture energy in friction, we can predict an unbounded friction coefficient at very small loads, governed by the geometry of the contacting body, thereby challenging oversimplified classical friction models. The actual friction coefficient at such minimal loads will depend on frictional behavior at the nanoscopic scale, which could be determined, for instance, through AFM measurements, as demonstrated by Peng et al. [25]. Our model employs only two parameters: the fracture energy for friction γ and the kinetic friction coefficient f, using the Griffith condition to determine the initiation of sliding, while actually assuming an infinite local static friction coefficient for the stick zone.

Extensive theoretical and experimental research has been devoted to the study of friction coefficients, notably by the group of Jay Fineberg, who have investigated transient rupture fronts propagating dynamically along frictional interfaces. Their work consistently demonstrates that fracture mechanics concepts remain applicable to friction, even under transient dynamic conditions [28–31]. Ben-David and Fineberg [31] demonstrated that friction coefficients can be significantly altered by minute changes in the loading geometry—on the order of a fraction of a degree—indicating that the friction coefficient may not be an intrinsic material property. Kammer et al. [32] applied linear elastic fracture

mechanics to friction problems to explain the observed nonlinearity in the growth of precursor lengths as a function of the applied force. Our model is fully consistent with the findings of the Fineberg group, particularly regarding the geometric dependence reported by Ben-David and Fineberg [31]. While their study focused on variations in punch inclination, we examine symmetrical indenter profiles and employ half-space theory to model the contact, making direct quantitative comparison with their experimental configuration infeasible. Moreover, as far as we understand, they did not study the influence of the normal load, leaving uncertain the limiting value of the ratio between static and dynamic friction coefficients.

Recently, Tada and Persson [33] reported that the global maximum static friction force F_B may not be a constant: its variation arises from the competition between local slip displacement λ_{el} and asperity size λ_{asp}. For slight local slip $\lambda_{el} \ll \lambda_{asp}$, global sliding requires breaking all asperity contacts simultaneously, thus the global static friction force reaches its maximum value. Conversely, when the local slip λ_{el} is large, asperity contacts are progressively broken and renewed during loading process, hence the global static friction force becomes equal to the dynamic friction force F_k. In addition to its dependence on surface roughness (the asperity size λ_{asp}), since the local slip is related to material deformation, the global maximum friction force also depends on the elastic modulus, sample size, and sliding velocity.

Our theory is based on a fracture energy, and as such, it requires a minimum size of contact area to be valid. For example, this scale may well be the 100 nm indicated by Gao and Yao [34] below which tips achieve their theoretical strength. This may prevent some of the points in the experiments of Peng et al. [25] to be correctly modeled. In this case, when contact becomes really that of very few asperities at nanoscale, the friction prediction of the AFM should be more appropriate, if available.

Although the present model predicts the dependence of the friction coefficient ratio on geometry, the available experimental data [25] can only validate the case of Hertzian geometry. This limitation could be addressed through future experimental validation based on power-law punch geometries.

5 Conclusion

We have demonstrated that, within the framework of the "Griffith" theory of friction, there can be very pronounced dependence of the ratio between static and dynamic friction coefficients on the contact geometry—contrary to classical friction theories, which assert that the friction coefficient is geometry independent. In particular, the model developed for 3D Hertzian punch is validated by experimental observations.

Our formulation incorporates the influence of the real contact area through a pressure-dependent frictional fracture energy. We have examined a power-law contact profile, as it provides a simple yet clear means of representing the transition from a more blunt to a flatter contact geometry. Many engineering and naturally occurring contacts closely approximate a flat geometry. Within our simplified friction model, the ratio of static to dynamic friction depends on the normal load as well as the power-law exponent: flatter profiles yield higher friction ratios, with the limiting value of this ratio potentially being very large. This characteristic may account for the considerable variability observed in experimentally reported friction coefficients. Furthermore, the geometric dependence derived here is based on a nondimensionalized quasi-static analysis, rendering the conclusions independent of elastic modulus, sample size, and loading rate.

Acknowledgment

M. C. acknowledges support from the Italian Ministry of Education, University and Research (MIUR) under the program Departments of Excellence (L.232/2016) and PRIN 2022 (Project ID: Prot.2022Y78C3K, CUP: D53C24004340006).

Conflict of Interest

There are no conflicts of interest.

Data Availability Statement

The datasets generated and supporting the findings of this article are obtainable from the corresponding author upon reasonable request.

Author Contribution Statement

Shubo Zhang: Formal analysis, methodology, software, validation, visualization, writing—original draft, and writing—review and editing. M. Ciavarella: Conceptualization, investigation, methodology, writing—original draft, and writing—review and editing.

Appendix: The Axisymmetric Power-Law Punch Solution

By assuming an axisymmetric power-law punch has the profile $g_0(r) = Cr^k$, we can derive the adhesiveless contact solution with equations (5.27) and (5.28) in the textbook by Barber [35]:

$$P = 2E^* \int_0^a \frac{r^2 g_0'(r)\,\mathrm{d}r}{\sqrt{a^2 - r^2}} = E^* Cka^{k+1} \mathrm{B}\left(\frac{k}{2} + 1, \frac{1}{2}\right)$$
$$\Delta = a \int_0^a \frac{g_0'(r)\,\mathrm{d}r}{\sqrt{a^2 - r^2}} = Cka^k \frac{1}{2} \mathrm{B}\left(\frac{k}{2}, \frac{1}{2}\right) \tag{A1}$$

The auxiliary function $h(t)$ and its derivative can be obtained by integrating equation (5.26) in the textbook by Barber [35]:

$$h(t) = \frac{E^*}{\pi}\left(t\int_0^t \frac{g_0'(r)\,\mathrm{d}r}{\sqrt{t^2 - r^2}} - \Delta\right) = \frac{E^*}{2\pi} Ck\mathrm{B}\left(\frac{k}{2}, \frac{1}{2}\right)(t^k - a^k)$$
$$h'(t) = \frac{E^*}{2\pi} Ck^2 \mathrm{B}\left(\frac{k}{2}, \frac{1}{2}\right) t^{k-1} \tag{A2}$$

The pressure distribution can be derived from equation (5.24) in the textbook by Barber [35]:

$$p(r) = \int_r^a \frac{h'(t)\,\mathrm{d}t}{\sqrt{t^2 - r^2}} = \frac{E^*}{2\pi} Ck^2 \mathrm{B}\left(\frac{k}{2}, \frac{1}{2}\right) a^{k-1} \cdot m_{k,3D}\left(\frac{r}{a}\right) \tag{A3}$$

where

$$m_{k,3D}(s) = \frac{1}{2}\Gamma\left(\frac{1-k}{2}\right) \cdot \left(\frac{\sqrt{\pi}}{\Gamma\left(1 - \frac{k}{2}\right)} s^{k-1} - {}_2\tilde{F}_1\left(\frac{1}{2}, \frac{1-k}{2}; \frac{3-k}{2}; s^2\right)\right) \tag{A4}$$

and $s = r/a \in [0, 1]$. Further, the regularized hypergeometric function ${}_2\tilde{F}_1$ is related to the Gaussian hypergeometric function by ${}_2\tilde{F}_1(a_1, a_2; b; z) = {}_2F_1(a_1, a_2; b; z)/\Gamma(b)$.

References

[1] Miron, A., Tadmor, R., Multanen, V., and Pinkert, S., 2025, "Da Vinci's Friction for Granular Media," Sci. Rep., **15**(1), p. 791.
[2] Rabinowicz, E., 1951, "The Nature of the Static and Kinetic Coefficients of Friction," J. Appl. Phys., **22**(11), pp. 1373–1379.
[3] Poliakov, A. N. B., Dmowska, R., and Rice, J. R., 2002, "Dynamic Shear Rupture Interactions With Fault Bends and Off-Axis Secondary Faulting," J. Geophys. Res.: Solid Earth, **107**(B11), p. ESE-6.
[4] Johnson, K., Kendall, K., and Roberts, A., 1971, "Surface Energy and the Contact of Elastic Solids," J. Phys. D: Appl. Phys., **6**(9), pp. 1017–1024.
[5] Ida, Y., 1972, "Cohesive Force Across the Tip of a Longitudinal-Shear Crack and Griffith's Specific Surface Energy," J. Geophys. Res., **77**(20), pp. 3796–3805.
[6] Palmer, A. C., and Rice, J. R., 1973, "The Growth of Slip Surfaces in the Progressive Failure of Over-Consolidated Clay," Proc. R. Soc. Lond. A. Math. Phys. Sci., **332**(1591), pp. 527–548.

[7] Maugis, D., and Barquins, M., 1978, "Fracture Mechanics and the Adherence of Viscoelastic Bodies," J. Phys. D: Appl. Phys., **11**(14), pp. 1989–2023.
[8] Savkoor, A. R., and Briggs, G. A. D., 1977, "The Effect of Tangential Force on the Contact of Elastic Solids in Adhesion," Proc. R. Soc. Lond. A. Math. Phys. Sci., **356**(1684), pp. 103–114.
[9] Rice, J. R., Lapusta, N., and Ranjith, K., 2001, "Rate and State Dependent Friction and the Stability of Sliding Between Elastically Deformable Solids," J. Mech. Phys. Solids., **49**(9), pp. 1865–1898.
[10] Ruina, A., 1983, "Slip Instability and State Variable Friction Laws," J. Geophys. Res.: Solid Earth, **88**(B12), pp. 10359–10370.
[11] Carpinteri, A., and Paggi, M., 2008, "Size-Scale Effects on Strength, Friction and Fracture Energy of Faults: A Unified Interpretation According to Fractal Geometry," Rock Mech. Rock Eng., **41**(5), pp. 735–746.
[12] Paggi, M., and Carpinteri, A., 2013, "Size-Scale Effects on the Friction Coefficient: From Weak Faults at the Planetary Scale to Superlubricity at the Nanoscale," *Recent Advances in Contact Mechanics: Papers Collected at the 5th Contact Mechanics International Symposium (CMIS2009), April 28–30, 2009, Chania, Greece*, G. E. Stavroulakis, ed., Springer, Berlin, Heidelberg, pp. 67–84.
[13] Cattaneo, C., 1938, "Sul Contatto Di Due Corpi Elastici: Distribuzione Locale Degli Sforzi," Rendiconti dell'Accademia Nazionale dei Lincei, **27**, pp. 342–348, 434–436, 474–478.
[14] Mindlin, R. D., 1949, "Compliance of Elastic Bodies in Contact," ASME J. Appl. Mech., **16**, pp. 259–268.
[15] Barenblatt, G., 1962, "The Mathematical Theory of Equilibrium Cracks in Brittle Fracture," Adv. Appl. Mech., **7**, pp. 55–129.
[16] Dugdale, D., 1960, "Yielding of Steel Sheets Containing Slits," J. Mech. Phys. Solids., **8**(2), pp. 100–104.
[17] Ciavarella, M., 1998, "The Generalized Cattaneo Partial Slip Plane Contact Problem. I—Theory," Int. J. Solids Struct., **35**(18), pp. 2349–2362.
[18] Ciavarella, M., 1998, "Tangential Loading of General Three-Dimensional Contacts," ASME J. Appl. Mech., **65**(4), pp. 998–1003.
[19] Jäger, J., 1998, "A New Principle in Contact Mechanics," ASME J. Tribol., **120**(4), pp. 677–684.
[20] Putignano, C., Ciavarella, M., and Barber, J. R., 2011, "Frictional Energy Dissipation in Contact of Nominally Flat Rough Surfaces Under Harmonically Varying Loads," J. Mech. Phys. Solids., **59**(12), pp. 2442–2454.
[21] Papangelo, A., and Ciavarella, M., 2015, "Cattaneo–Mindlin Plane Problem With Griffith Friction," Wear, **342–343**, pp. 398–407.
[22] Papangelo, A., Ciavarella, M., and Barber, J. R., 2015, "Fracture Mechanics Implications for Apparent Static Friction Coefficient in Contact Problems Involving Slip-Weakening Laws," Proc. R. Soc. A: Math., Phys. Eng. Sci., **471**(2180), p. 20150271.
[23] Griffith, A. A., 1921, "The Phenomena of Rupture and Flow in Solids," Phil. Trans. R. Soc. Lond. Ser. A, Contain. Pap. Math. Phys. Charact., **22**, pp. 163–198.
[24] Ciavarella, M., 2015, "Transition From Stick to Slip in Hertzian Contact With "Griffith" Friction: The Cattaneo–Mindlin Problem Revisited," J. Mech. Phys. Solids., **84**, pp. 313–324.
[25] Peng, L., Roch, T., Bonn, D., and Weber, B., 2025, "Decrease of Static Friction Coefficient With Interface Growth From Single to Multiasperity Contact," Phys. Rev. Lett., **134**(17), p. 176202.
[26] Ciavarella, M., 2025, "On the Dependence of Static Friction Coefficient on Normal Load," Tribol. Lett., **73**(4), p. 130.
[27] Xu, Y., Scheibert, J., Gadegaard, N., and Mulvihill, D. M., 2022, "An Asperity-Based Statistical Model for the Adhesive Friction of Elastic Nominally Flat Rough Contact Interfaces," J. Mech. Phys. Solids., **164**, p. 104878.
[28] Svetlizky, I., and Fineberg, J., 2014, "Classical Shear Cracks Drive the Onset of Dry Frictional Motion," Nature, **509**(7499), pp. 205–208.
[29] Ben-David, O., Cohen, G., and Fineberg, J., 2010, "The Dynamics of the Onset of Frictional Slip," Science, **330**(6001), pp. 211–214.
[30] Ben-David, O., Rubinstein, S. M., and Fineberg, J., 2010, "Slip-Stick and the Evolution of Frictional Strength," Nature, **463**(7277), pp. 76–79.
[31] Ben-David, O., and Fineberg, J., 2011, "Static Friction Coefficient Is Not a Material Constant," Phys. Rev. Lett., **106**(25), p. 254301.
[32] Kammer, D. S., Radiguet, M., Ampuero, J. -P., and Molinari, J. -F., 2015, "Linear Elastic Fracture Mechanics Predicts the Propagation Distance of Frictional Slip," Tribol. Lett., **57**(3), p. 23.
[33] Tada, T., and Persson, B. N. J., 2025, "On the Origin of the Breakloose Friction Force," J. Chem. Phys., **162**, p. 174709.
[34] Gao, H., and Yao, H., 2004, "Shape Insensitive Optimal Adhesion of Nanoscale Fibrillar Structures," Proc. Natl. Acad. Sci. USA, **101**(21), pp. 7851–7856.
[35] Barber, J., 2018, *Contact Mechanics* (Solid Mechanics and Its Applications), Springer International Publishing, Cham.